3rd European supercritical CO2 Conference
September 19-20, 2019, Paris, France

2019-sCO2.eu-156

# PART-LOAD OPERATION OF COAL FIRED SCO2 POWER PLANTS

**Dario Alfani***
Politecnico di Milano
Milano, Italy
Email: dario.alfani@polimi.it

**Marco Astolfi**
Politecnico di Milano
Milano, Italy

**Marco Binotti**
Politecnico di Milano
Milano, Italy

**Ennio Macchi**
Politecnico di Milano
Milano, Italy

**Paolo Silva**
Politecnico di Milano
Milano, Italy

## ABSTRACT

The present work deals with the study of the part-load performance and operating strategies of a coal fired $sCO_2$ power plant. In $sCO_2$ cycles the compression phase generally starts very close to the fluid critical point in a region characterized by significant real gas effects, so that depressurization, that is the typical operating strategy adopted for closed gas cycles, may not be the optimal one. In fact, a significant variation of fluid thermodynamic properties along the compression will occur with a probable penalization on the overall plant efficiency. A recuperative recompressed cycle with High Temperature Recuperator (HTR) achieving a cycle efficiency of 41.92% is designed and part-load performances of the overall power plant are analyzed also taking into account the boiler off-design behavior. Different operating strategies are investigated considering the combinations of component features such as rotational speed and variable geometry at the inlet of turbomachinery, fan speed on the heat rejection unit, variation of the fluid inventory. The best operating strategy energy-wise is finally proposed, providing a numerical estimation of the off-design overall plant performance and highlighting some design criteria for boiler and turbomachinery.

## INTRODUCTION

Supercritical $CO_2$ cycles for power generation are gaining a large interest from industry, institutions and academia as demonstrated by the large amount of investments, founded projects and research papers. This attention is motivated by the potential of $sCO_2$ technology of replacing conventional steam plants in a number of applications and likely playing a relevant role in the future energy scenario. The H2020 sCO2-Flex [1] project is studying the possible application of $sCO_2$ cycles in coal fired power plants in order to enhance their flexibility and ease the integration with non-dispatchable renewable energy sources such as wind and solar. Main advantages of $sCO_2$ power plants with respect to USC technology are: (i) potential higher efficiency, (ii) compactness of the turbomachinery, (iii) no need of water treatment, deaerator, vacuum pump, etc., (iv) high performance at part-load and (v) fast transients. The first two figures have been numerically evaluated in different independent studies while the assessment of flexibility still lacks deep investigation. This study focuses on the part-load performance and control strategies for a $sCO_2$ cycle used as power cycle in a coal-fired power plant. Differently from closed Joule-Brayton cycles using for example He and $N_2$ that operate in the ideal gas region, in $sCO_2$ power cycles the main compressor is generally designed to operate very close to the fluid critical point in a region characterized by marked real gas effects (i.e. a region where the gas has a compressibility factor $Z$ significantly lower than 1) [2]. For these plants, cycle depressurization at partial load may involve a significant variation of fluid properties along compression with an efficiency penalization that may jeopardize also the overall plant performance. The optimization of the part-load operation of $sCO_2$ power plants is scarcely studied in literature and the main unknowns regard the design and the operation of turbomachinery. Different operating strategies are investigated in this work for a recuperative recompressed cycle configuration selected within the sCO2-Flex project and considering the combinations of component features: (i) turbine and compressor (fixed/variable velocity, with or without variable geometry), (ii) heat rejection unit (fixed/variable fan speed), (iii) fluid inventory (variable/fixed). For each design combination, the best operating strategy in terms of system efficiency is proposed, providing a numerical estimation of the part-load performance attainable with $sCO_2$ power plants and highlighting suggested design criteria for the turbomachinery.

* corresponding author



DOI: 10.17185/duepublico/48897

## METHODOLOGY AND CYCLE LAYOUT

Due to the large number of possible applications for $sCO_2$ cycles, more than 50 different $sCO_2$ cycle layouts have been proposed in literature [3]. The use of a $sCO_2$ cycle as power cycle for coal-fired power plants is being investigated within the sCO2-Flex project which has identified 21 promising cycles for this specific application. Typically, $sCO_2$ cycles are strongly regenerative, limiting the temperature variation across the primary heat exchanger: this feature allows achieving high cycle efficiencies, but does not ease the coupling with a boiler in which it is necessary to cool down as much as possible the hot flue gases. Combustion air preheating by means of a Ljungström heat exchanger can mitigate this problem, but a compromise between cycle and boiler efficiency is required. After a preliminary analysis, the sCO2-Flex consortium has identified three cycles as the most suitable ones for the selected application. The selection was made considering i) the cycle performance, ii) the boiler integration and performance and iii) the system simplicity. In this study a recuperative recompressed cycle with High Temperature Recuperator (HTR) bypass is considered. The cycle layout is reported in Fig. 1.

This cycle is the simplest among the three cycles selected within the sCO2-Flex project [4] and guarantees effective flue gas cooling thanks to the $CO_2$ stream that bypasses the HTR and is heated up in the boiler. The presence of the secondary compressor allows a good balance of the heat capacities of the cold and hot $CO_2$ streams in the Low Temperature Recuperator (LTR), reducing the irreversibilities related to the heat exchange and thus boosting the cycle efficiency.

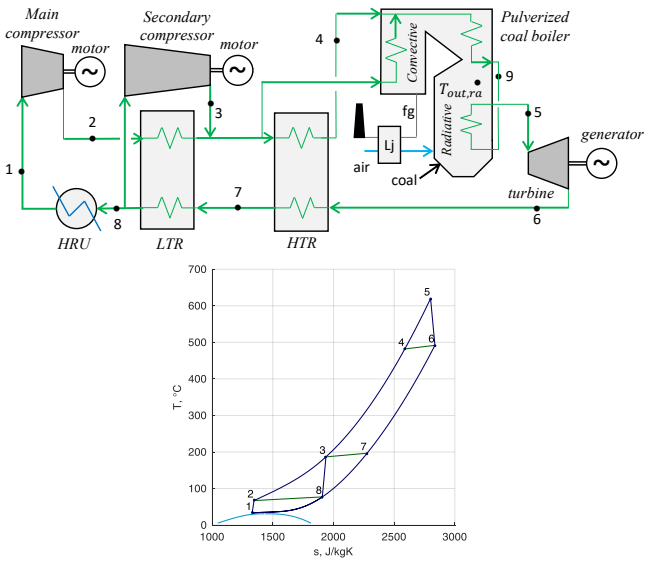


**Figure 1:** (top) schematic plant layout and (bottom) T-s diagram of the recompressed cycle with HTR bypass.

The numerical model adopted within sCO2-Flex and used in this work for the simulation of the coal-fired $sCO_2$ power plant has been developed in MATLAB® [5] and adopts REFPROP 9.1 database [6] for the calculation of thermodynamic properties of $CO_2$. The code is able to solve mass and energy balances, to compute the cycle thermodynamic performances and to evaluate the main components design parameters for several cycle configurations.

Once the design is performed, the obtained results (e.g. heat exchanger surfaces and volumes) are used as input data for the part-load simulation. The different part-load operating strategies are compared in terms of system efficiency and turbomachinery operating conditions, neglecting in this phase of the study the variation of the turbomachinery efficiency.

## CYCLE THERMODYNAMIC DESIGN

The analysis in the present study is carried out for a power plant having a gross cycle electric power output ($\dot{W}_{gross}$) of 100 $MW_{el}$. Cycle maximum temperature and pressure are set to 620°C and 250 bar respectively, according to the current values used for Ultra Super Critical (USC) boilers. Turbine efficiency and compressor efficiencies were evaluated with a preliminary sizing in [7]. In order to ease the replicability of the system in different sites an air-cooled heat rejection unit is considered. The minimum cycle temperature is fixed to 33°C, while the minimum cycle pressure is optimized in order to maximise the cycle efficiency. As further assumption, the same temperature is assumed for the high-pressure $CO_2$ stream exiting the LTR and for the $CO_2$ stream exiting the secondary compressor, thus guaranteeing no mixing losses. Similarly, the high-pressure $CO_2$ exiting the HTR and the bypass $CO_2$ stream are isothermally mixed. All the main assumptions for the cycle design are summarized in Table 1.

**Table 1:** Main assumptions for the cycle design

| **Cycle assumptions** | |
|---|---|
| Cycle design gross electric power $W_{gross}$, MW | 100 |
| Maximum cycle temperature $T_5$,°C | 620 |
| Maximum cycle pressure $p_2$, bar | 250 |
| Minimum cycle temperature $T_1$,°C | 33 |
| Turbine isentropic efficiency, $\eta_{turb}$ | 84.3 % * |
| Main compressor isentropic efficiency, $\eta_{comp1}$ | 82.2 % * |
| Second. compressor isentropic efficiency $\eta_{comp2}$ | 82.4 % * |
| Generator/motor efficiency $\eta_{me,t}$/ $\eta_{me,c}$ | 96.4 % |
| LTR pinch point $\Delta T_{LTR}$,°C | 10 |
| HTR pinch point $\Delta T_{HTR}$,°C | 10 |
| HRU $CO_2$ $(\Delta p/p_{in})$ | 0.5 % |
| Recuperator hot side $(\Delta p/p_{in})$ | 0.5 % |
| Recuperator cold side $(\Delta p/p_{in})$ | 0.5 % |
| HRU electric cons. per MW of heat rejected $\xi$ | 0.0085 |

*The reported turbomachinery efficiency value is just indicative.

Cycle thermodynamic efficiency ($\eta_{cycle}$) is calculated considering the turbine and compressors work, the mechanical and electric efficiencies of generator ($\eta_{me,t}$) and motors ($\eta_{me,c}$) and the heat rejection auxiliaries consumption.

$$\eta_{cycle} = \frac{\dot{W}_{net}}{\dot{Q}_{in,cycle}} = \frac{\dot{W}_t - \dot{W}_{c1} - \dot{W}_{c2} - \dot{W}_{HRU,aux}}{\dot{Q}_{in,cycle}} = \frac{\left[\Delta h_{5-6}\eta_{me,t} - SR\frac{\Delta h_{1-2}}{\eta_{me,c}} - (1-SR)\frac{\Delta h_{3-8}}{\eta_{me,c}} - SR\xi\Delta h_{8-1}\right]}{\Delta h_{4-5} + BR\,\Delta h_{3-4}} \quad (1)$$



DOI: 10.17185/duepublico/48897

## BOILER THERMODYNAMIC DESIGN

The boiler is fuelled with BILINA HP1 coal, whose ash-free chemical composition on a molar basis is C: 37.85%, H: 34.81%, O: 9.16%, N: 0.40%, S: 0.25%, $H_2O$: 17.53% with a Lower Heating Value (LHV) equal to 16.9 MJ/kg. Closed system coal drying is assumed, thus evaporated water enters the boiler together with coal and flue gas composition corresponds to coal as received. The excess of air with respect to the stoichiometric value is assumed equal to 20% in order to guarantee complete combustion and to limit boiler stack losses. The stack temperature has been limited to 130°C in order to avoid acid condenses in the flue gases, mainly caused by the combination of sulfur trioxide ($SO_3$) present in the flue gases with moisture to form sulfuric acid ($H_2SO_4$). The adiabatic flame temperature is computed for simplicity without considering air staging, as this has secondary impact on the overall boiler energy balance.

The heat exchangers layout in the boiler is preliminary and considers two different boiler zones:

- A high temperature radiative zone where the main heat exchange mechanism is the radiation due to the presence of the flame and the high temperature of the flue gases. This zone includes the high temperature section of the Primary Heat Exchanger (HT-PHE) and the flue gases are cooled down to 1200°C [8].
- An intermediate-low temperature radiative-convective zone in which both radiation and convection are considered. In this zone the low temperature section of the Primary Heat Exchanger (LT-PHE) and the HTR bypass heat exchanger (HTRB) are considered.

**Table 2:** Main assumptions for the boiler thermodynamic design

| **Boiler assumptions** | |
|---|---|
| Ambient temperature, °C | 20 |
| Minimum allowable stack temperature $T_{stack}$,°C | 130 |
| Minimum allowable boiler pinch point $\Delta T_{pp,boiler}$,°C | 50 |
| Minimum allowable Ljungström pinch point $\Delta T_{pp,Lj}$,°C | 30 |
| Boiler $CO_2$ side $\Delta p_{boiler}$, bar | 2.5 |
| Excess of air | 20% |
| Flue gas temperature at the radiative zone exit, $T_{out,rad}$, °C | 1200 |
| Maximum air temperature at LJ outlet, $T_{LJ,max}$, °C | 350 |

Boiler efficiency ($\eta_{boiler}$) is calculated considering the heat loss with the flue gases at the stack, thus neglecting heat losses from boiler walls to the environment:

$$\eta_{boiler} = \frac{\dot{Q}_{in,cycle}}{\dot{Q}_{LHV}} = 1 - \frac{\int_{T_{amb}}^{T_{stack}} \dot{m}_{fg} c_{p,fg}(T) dT}{\dot{m}_{fuel} LHV_{fuel}} \quad (2)$$

The plant overall efficiency ($\eta_{plant}$) is calculated as the product between cycle efficiency and boiler efficiency:

$$\eta_{plant} = \eta_{cycle}\eta_{boiler} = \frac{\dot{W}_{net}}{\dot{Q}_{LHV}} \quad (3)$$

## HEAT EXCHANGERS SIZING

The detailed design of the heat exchangers is performed according to the thermodynamic design of the cycle and of the boiler, assuming the pressure drops provided in Table 1 as target.

As widely suggested in literature [9][10][11], Printed Circuit Heat Exchangers (PCHE) are considered for the LTR and HTR and their sizing is made in accordance with the work developed by Dostal [9] and with a set of hypotheses already used in previous works [4][12]. The recuperators are discretized in 50 sections and for each segment the overall heat transfer coefficient, the required heat transfer area, metal and $sCO_2$ volumes are obtained.

The primary heat exchanger is designed as a two-pass heat exchanger. The radiative high temperature section (HT-PHE) is considered as a membrane wall heat exchanger while the convective-radiative intermediate temperature section (LT-PHE) is assumed as counter flow tubular heat exchanger. The HTRB heat exchanger is assumed as a counter flow tubular heat exchanger as well. The value of the radiative heat flux on the membrane walls is computed through a series of Thermoflex [8] simulations of the radiant boiler component and its value is assumed equal to 117 kW/m$^2$.

Both tubular heat exchangers in the boiler (LT-PHE and HTRB) are discretized in 50 steps, each one exchanging the same amount of heat. The internal heat transfer coefficient is computed with the Dittus-Boelter correlation [13], while the external heat transfer coefficient is computed as the sum of a convective and a radiative contribution, both estimated through correlation obtained from Thermoflex as function of the flue gases velocity and temperature[8], [12].

The overall heat transfer coefficient referred to the internal area for the $j$-th step $U_{in,j}$ is then obtained as:

$$U_{in,j} = \left( \frac{1}{htc_{CO2,j}} + \frac{d_{in} \ln\left(\frac{d_{ex}}{d_{in}}\right)}{2k_t} + \frac{\frac{A_{in,j}}{A_{ex,j}}}{(htc_{FG,rad} + htc_{FG,conv})} \right)^{-1} \quad (4)$$

The internal heat transfer area of each heat exchanger in the radiative-convective section is finally computed as:

$$A_{in} = \sum_{j=1}^{50} \frac{\dot{Q}_j}{U_{in,j} \Delta T_{ml,j}} \quad (5)$$

The heat rejection unit heat exchange area is predicted with LU-VE proprietary correlations [14] computing the heat transfer coefficients, the pressure drops and the overall heat exchanger area.

Finally, the Ljungström air preheater, given its effectiveness from the thermodynamic design, is sized with Thermoflex.

The main geometrical assumptions for the different heat exchangers design are reported in Table 3.


DOI: 10.17185/duepublico/48897

**Table 3:** Main assumptions for the different heat exchangers design

| | |
|---|---|
| **PCHE** | |
| Thickness of plate, mm | 1.5 |
| Diameter of semi-circular channel, mm | 2 |
| Thickness of wall between channels, mm | 0.4 |
| Heat exchanger material | INCOLOY 800 |
| **HT-PHE** | |
| Tube internal diameter, mm | 20 |
| Ratio of tube pitch to external diameter | 1.45 |
| Tube and membrane material | INCONEL 617 |
| **HTRB and LT-PHE** | |
| Tube internal diameter, mm | 40 |
| Ratio of tube pitch to external diameter | 1.2 |
| Ratio of transverse tube pitch to ext. diameter | 10 |
| Tube material | INCONEL 617 |

## DESIGN RESULTS

The results of the thermodynamic design of the system are reported in Table 5. The obtained net cycle efficiency is 41.92%, while the boiler efficiency is 94.37%; combining these two contributions an overall efficiency of 39.56% is achieved. All the main thermodynamic properties of the cycle streams are reported in Table 4.

**Table 4:** Thermodynamic streams of the $sCO_2$ cycle

| Point | Temp. (°C) | Press. (bar) | Density (kg/m³) | Enthalpy (kJ/kg) | Entropy (kJ/kgK) |
|---|---|---|---|---|---|
| 1 | 33 | 81.18 | 632.40 | 301.77 | 1.33 |
| 2 | 67.13 | 250 | 751.30 | 330.74 | 1.34 |
| 3 | 186.68 | 248.75 | 343.45 | 563.33 | 1.94 |
| 4 | 481.88 | 247.51 | 167.71 | 946.82 | 2.59 |
| 5 | 620 | 245.51 | 138.39 | 1120.15 | 2.80 |
| 6 | 491.88 | 82.41 | 56.60 | 974.91 | 2.84 |
| 7 | 196.68 | 81.99 | 99.65 | 635.15 | 2.28 |
| 8 | 77.13 | 81.58 | 168.38 | 485.70 | 1.91 |
| 9 | 531.14 | 246.80 | 155.81 | 1008.4 | 2.67 |

As it is possible to notice from Figure 2, which depicts the boiler T-Q diagram, the optimal boiler design presents values of pinch point temperature differences at the main HX sections higher than the minimum achievable technical value. This fact is due to the limitation imposed to the stack temperature and to the combustion air preheating temperature.

Thus, as it is possible to notice from Table 5 that, in order to maximize the boiler efficiency, stack temperature is pushed down by the optimizer to its lower bound value, while at the same time the air combustion temperature at Ljungstrom HX exit is pushed to its upper bound value.

**Table 5:** Main results of the boiler and cycle design.

| **Boiler and cycle optimized results** | |
|---|---|
| $CO_2$ mass flow at turbine inlet, kg/s | 1087.12 |
| $CO_2$ mass flow at HRU, kg/s | 698.53 |
| $CO_2$ mass flow at HTR bypass, kg/s | 123.95 |
| Split ratio SR | 0.643 |
| Bypass ratio BR | 0.114 |
| Minimum cycle pressure $p_1$, bar | 81.18 |
| Coal mass flow rate, kg/s | 14.80 |
| Air mass flow rate, kg/s | 98.22 |
| Flue gases mass flow rate, kg/s | 111.65 |
| Adiabatic flame temperature, °C | 1980.96 |
| Flue gases stack temperature, °C | 130 |
| Optimal boiler pinch point $\Delta T_{pp,boiler}$,°C | 209.25 |
| Ljungström pinch point $\Delta T_{pp,Lj}$,°C | 45.93 |
| Turbine electric power, $MW_{el}$ | 152.27 |
| Main compressor electric power, $MW_{el}$ | 20.98 |
| Secondary compressor electric power, $MW_{el}$ | 31.28 |
| Heat rejection auxiliaries consumption, $MW_{el}$ | 1.09 |
| **Cycle efficiency** | **41.92%** |
| **Boiler efficiency** | **94.37%** |
| **Overall efficiency** | **39.56%** |

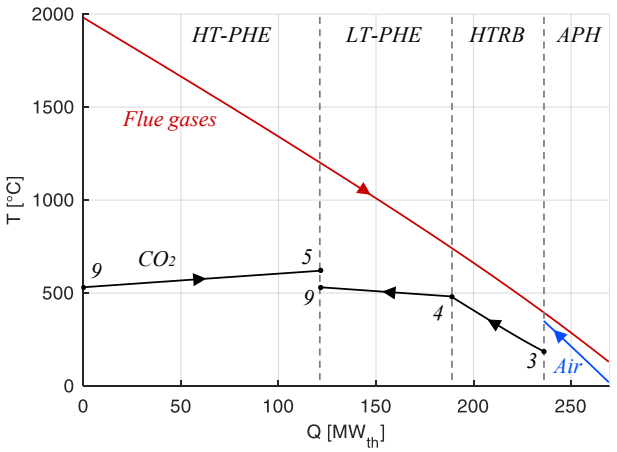


**Figure 2:** Boiler T-Q (temperature vs. thermal power exchanged) diagram.

Table 6 reports the main results of the HX design showing how the two recuperators require large overall heat exchange areas due to the small $\Delta T_{LTR}$ and $\Delta T_{HTR}$ selected.

**Table 6:** Main results of the heat exchangers design

| Parameter | HRU | LTR | HTR | HT-PHE | LT-PHE | HTRB |
|---|---|---|---|---|---|---|
| Heat duty, MW | 188.4 | 162.4 | 369.3 | 121.5 | 66.9 | 47.5 |
| Hot side heat transfer coefficient, W/m²K | 4880.7 | 4398.9 | 3682.7 | - | 105.7 | 84.7 |
| Cold side heat transfer coefficient, W/m²K | 75.8 | 4503.5 | 3717.4 | - | 3419.6 | 4247.1 |
| Global heat transfer coefficient, W/m²K | 53.4 | 2039.5 | 1737.6 | 80.2 | 98.2 | 80.3 |
| Internal heat transfer surface, m² | 8912 | 6898.7 | 14345.5 | 1595 | 1203 | 1876 |
| HX metal mass, kg | 70316 | 43258 | 89953 | 77331 | 73573 | 113787 |



DOI: 10.17185/duepublico/48897

## PART LOAD OPERATION

The analysis of the system at part load is performed assuming a reduction of the fuel input and a proportional reduction of the combustion air to keep the air-to-fuel ratio constant and to guarantee an effective combustion also in off-design conditions. For the considered preliminary analysis, a constant ambient air temperature and a constant compressor inlet temperature are assumed as well, since the focus of the work is on the different operating strategies available for an active part-load control. As in design conditions, an isothermal mixing at the high pressure exit of the LTR and HTR is imposed by properly varying the split fraction to the secondary compressor and the one to the HTR bypass. The maximum $sCO_2$ temperature ($T_5$) is kept constant in order to simplify the analysis and avoid metal overheating in the furnace. The pressure drops in each heat exchanger section at part-load are corrected with respect to the design value through the following correlation:

$$\Delta p = \Delta p_{design} \left(\frac{\rho_{design}}{\rho}\right) \left(\frac{\dot{m}}{\dot{m}_{design}}\right)^2 \quad (6)$$

The heat transfer coefficients at part load operation on the $CO_2$ side for LTR, HTR, HTRB and LT-PHE and on the flue gas side for HTRB and LT-PHE are computed with a simplified approach as function of the ratio between the mass flow rate in off-design conditions and the mass flow rate in nominal operation:

$$htc_{CO2} = htc_{CO2,design} \left(\frac{\dot{m}_{CO2}}{\dot{m}_{CO2,design}}\right)^{0.8} \quad (7)$$

$$htc_{FG} = htc_{FG,design} \left(\frac{\dot{m}_{FG}}{\dot{m}_{FG,design}}\right)^{0.6} \quad (8)$$

The different exponents on the mass flow ratios for $CO_2$ and flue gases depends on the different correlations used for the calculation of the convective heat transfer coefficients [13].

In the HT-PHE, being the radiation the main heat exchange mechanism, the equivalent overall heat transfer coefficient $U_{ra}$ computed in nominal conditions (see

Table 6) is kept constant independently from the load as the variation of the adiabatic flame temperature is limited.
Finally, for the HRU, it has been preferred to adopt ad hoc correlations due to the proximity of the $CO_2$ thermodynamic conditions to the critical point [15].

Heat rejection unit fan consumption is calculated with reference to the nominal value and adopting an exponential function as reported:

$$\dot{W}_{HRU,aux} = \dot{W}_{HRU,aux,design} \left(\frac{\dot{m}_{air}}{\dot{m}_{air,design}}\right)^{2.78} \quad (9)$$

Different options are available for the part-load control of the cycle, depending on the turbomachinery features: compressors and turbine may be equipped with Variable Inlet Guide Vanes (VIGV) and may be able to vary their rotational speed. Moreover, a further option available in closed gas cycles is related to the possibility of varying the working fluid inventory thus changing the operating pressure of the system. In the present work different options are considered for the $sCO_2$ turbine and their effect on cycle performance and compressors operating points are investigated. The turbine is assumed to operate in chocked flow conditions, thus the following correlation holds:

$$\frac{\dot{m}_5\sqrt{T_5}}{p_5 A_{in,turb}} = \frac{\dot{m}_{5,design}\sqrt{T_{5,design}}}{p_{5,design} A_{in,turb,design}} \quad (10)$$

For simplicity, no variation on turbomachinery efficiency is considered. The following cases are identified:

- CASE 1: Turbine in sliding pressure and fixed minimum cycle pressure;
- CASE 2: Turbine in sliding pressure and optimized variable minimum cycle pressure;
- CASE 3: Turbine with partial admission and fixed minimum cycle pressure.

## RESULTS

*CASE 1: Turbine in sliding pressure and fixed minimum cycle pressure.*

Figure 3, left depicts the trend of cycle efficiency, boiler efficiency and the plant efficiency. The cycle efficiency tends to remain constant for a wide range of fuel input as the negative effect related to the reduced compression ratio with consequent reduction of the net specific power output of the cycle is compensated by the increased heat exchangers effectiveness. In fact, at part load the heat exchangers are oversized with respect to their duty and thus perform in a more effective way as it is possible to see from the boiler efficiency trend. For coal mass flow rates below 60% of the nominal value cycle efficiency drops due to the excessive decrease in the pressure ratio of the cycle. Furthermore, the strong reduction of the $CO_2$ mass flow rates penalizes the HX heat transfer coefficients limiting the internal heat regeneration of the cycle.

Figure 3, right reports the trends of the adiabatic flame temperature and flue gases stack temperature: as the coal mass flow rate is reduced and the $CO_2$ is able to cool down the flue gases in a more efficient manner, the heat available for air preheating decrease thus limiting the combustion air temperature and consequently the adiabatic flames temperature. At very low loads these effects are limited by the strong penalization of the HXs heat transfer coefficients due to the reduced mass flow rates.


DOI: 10.17185/duepublico/48897

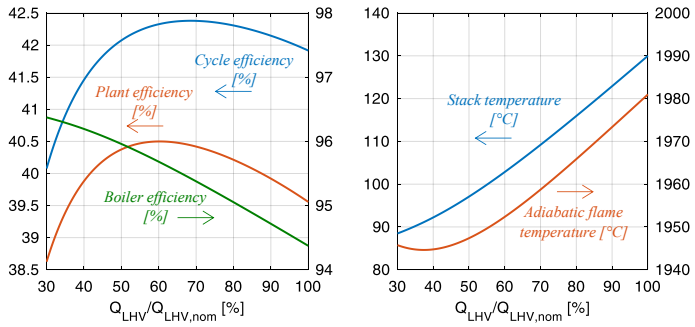


**Figure 3:** (left) Trends of the cycle efficiency, boiler efficiency and plant efficiency as function of the boiler heat input and (right) stack and adiabatic flame temperature as function of the fuel input for CASE 1.

*CASE 2: Turbine in sliding pressure and optimized variable minimum cycle pressure.*

The previous analysis strongly highlights how at lower loads could be beneficial to increase the cycle pressure ratio in order to limit the penalization on cycle efficiency and power plant net power output. This kind of regulation can be obtained with different compressor features: a possibility is the adoption of VIGV at compressors inlet and/or to employ electrical motors equipped with frequency converters to vary the rotational speed of the turbomachines.

A sensitivity analysis is carried out decreasing the minimum cycle pressure (equal to 81.18 bar in design conditions) with a step of 1 bar with respect to the nominal one in order to have six different scenarios. Figure 4 depicts the trend of the plant efficiency: it is possible to note that optimal minimum pressure decreases with the fuel input thanks to the increased pressure ratio leading to a higher net specific power output. Acting properly on the cycle minimum pressure allows in the case of 30% coal mass flow rate to slightly increase the efficiency from a value equal to 38.62% up to a value of 39.35%.

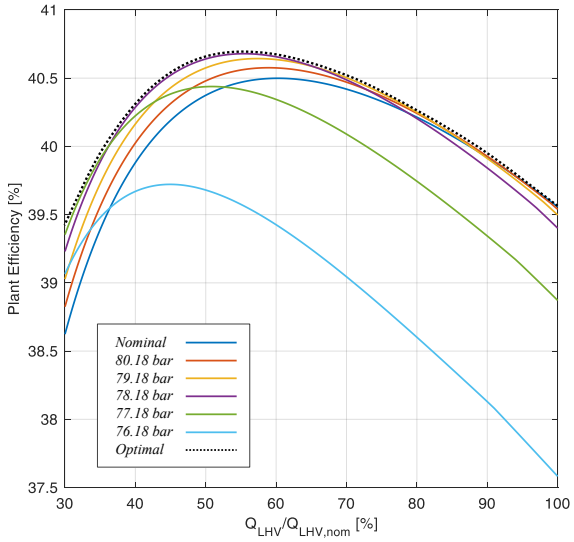


**Figure 4:** Trends of the plant efficiency as function of the fuel input for different minimum cycle pressures (CASE 2).

Figure 5 and Figure 6 report the main and the secondary compressor operating points as function of the fuel input for CASE 1 and CASE 2 on a dimensionless $\Delta h - \dot{V}$ chart. The white areas on the charts show the operating region for the two compressors equipped with VIGV and variable speed (60%/105%) according to a preliminary design performed within the sCO2-Flex project: line on the top-left represents the surge limit, while line on the bottom-right represents the choke limit. In CASE 1, at minimum fuel input (30%) the main compressor operating point falls out of the operative region crossing the surge limit line while in CASE 2 this is avoided. In fact, decreasing the minimum pressure with the load allows to walk off the critical point limiting the reduction of the volumetric flow (the compressibility factor at the compressor inlet and the SR increase) not incurring in any issue related to choking or surge. The operating points of the secondary compressor reported in Figure 6 do not show particular criticalities and do not impose further constrains to the operation of the system. Differently from the primary compressor, the secondary compressor at minimum fuel input and for reduced minimum pressure experiences a reduction of the inlet volumetric flow mainly due to the reduction of its mass flow rate, proportional to (1-SR). One further degree of freedom not investigated in this work is related to the possibility of varying the split ratio SR removing the isothermal mixing constraint and thus act both on the main and secondary compressor volumetric flows. It is important to underline once again that a more detailed investigation considering also the variation of turbomachinery isentropic efficiency is necessary to evaluate the best operating strategy at part load.

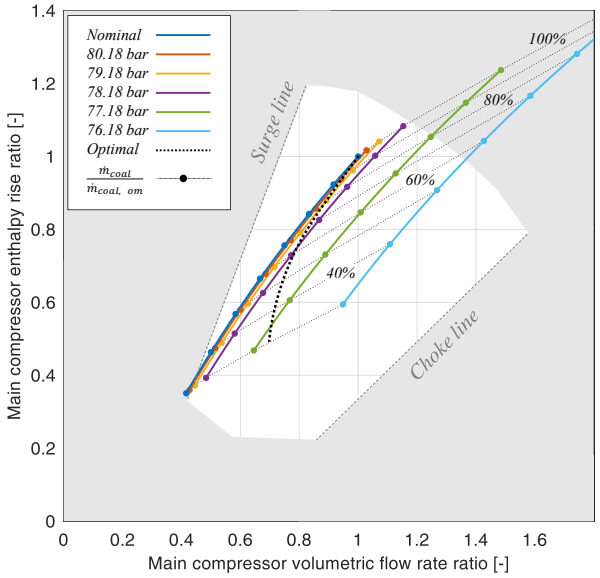


**Figure 5:** Main compressor operating points for the fixed minimum cycle pressure equal to the nominal value (CASE 1) and for variable minimum pressure case (CASE 2) as function of the fuel input. The white area in the figure represents the operating region for the main compressor with VIGV and variable rotating speed.



DOI: 10.17185/duepublico/48897

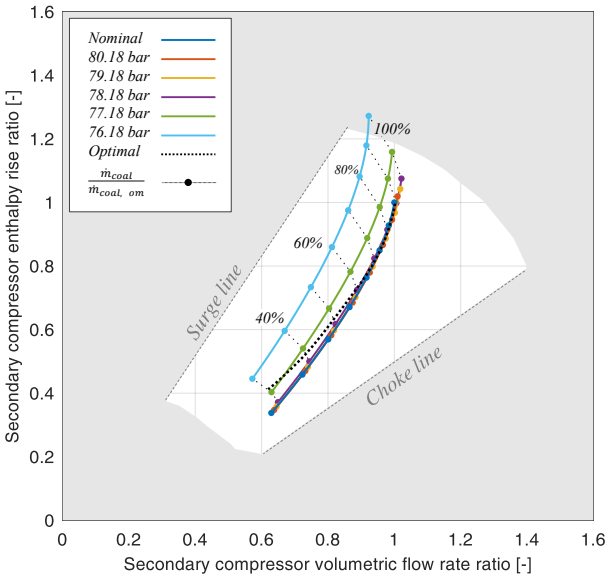


**Figure 6:** Secondary compressor operating points for the fixed minimum cycle pressure equal to the nominal value (CASE 1) and for variable minimum pressure case (CASE 2) as function of the fuel input. The white area in the figure represents the operating region for the main compressor with VIGV and variable rotating speed.

*CASE 3: Turbine with partial admission and fixed minimum cycle pressure.*

A further possibility in order to control part-load operation of $sCO_2$ power plants is to provide the turbine by Inlet Guide Vanes (IGV) or a partial admission arc in order to control the cycle maximum pressure. The choice between the two technologies generally depends mainly on the size and the type of the component (radial centripetal vs axial turbine) and on its maximum operating temperature, factors that can significantly limit the adoption of these technologies due to the high thermomechanical stresses. The analysis is repeated only for the nominal value of the cycle minimum pressure assuming a fixed value of the maximum cycle pressure, but the analysis can be extended combining the contribution of the different control strategies. Figure 7 shows how the plant efficiency for CASE 3 increases thanks to the improved effectiveness of the heat exchangers. At 30% of the fuel input the plant efficiency achieves 41.76%, 2.41 percentage points more than CASE 2. However, a severe drawback of this control strategy is related to the compressors operating point (see Figure 8): already at 80-90% of the coal fuel input the operating point of the compressors moves towards the surge zone, crossing it for a value around the 75% of the load. This fact not only limits significantly the initial hypothesis on constant turbomachinery efficiency, but it makes impossible to adopt this strategy in order to control the plant at partial loads.

A possible solution is the use of more compressors in parallel that can be switched off as the load is reduced. It is important to underline anyhow that smaller compressors may be characterized by lower performance and higher total costs. Another solution is related to the selection of a different design point of the compressor. Finally, as for the sliding pressure case, a variation of the minimum cycle pressure can positively influence the volumetric flow at the compressor inlet.

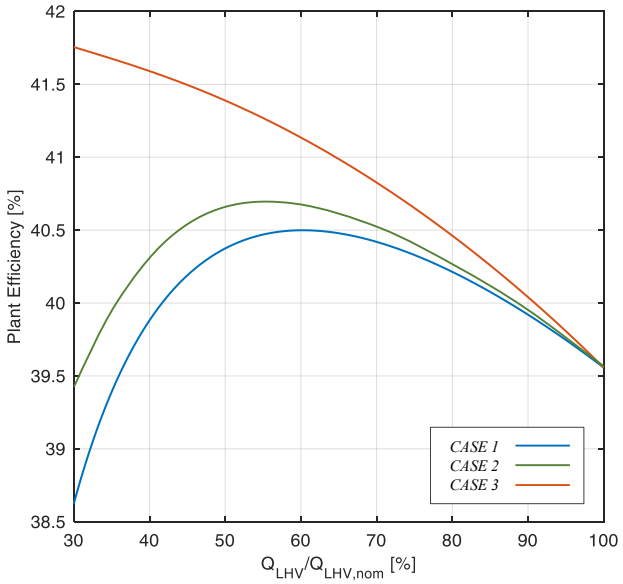


**Figure 7:** Variation of plant efficiency with the fuel input for the three different investigated strategies

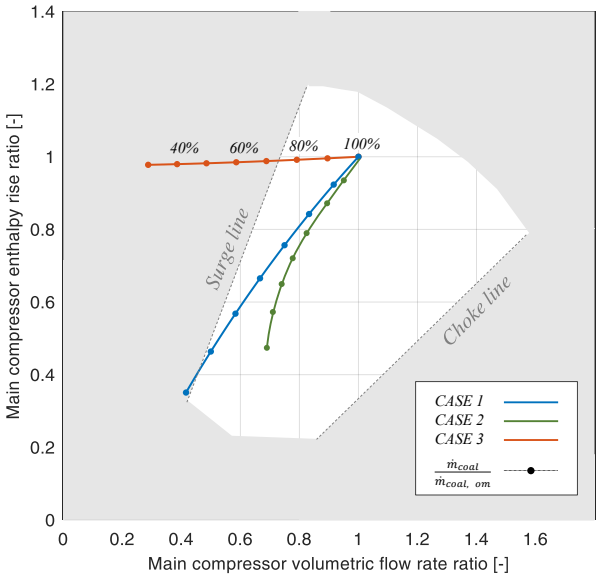


**Figure 8:** Main compressor operating points for CASE 1, CASE 2 and CASE 3 as function of the fuel input. The white area in the figure represents the operating region for the main compressor with VIGV and variable rotating speed.


DOI: 10.17185/duepublico/48897

## CONSIDERATIONS ON $CO_2$ INVENTORY

From the design of each heat exchanger and assuming reasonable piping length between the different components the inventory of $CO_2$ was computed in nominal conditions and at part load for the three different studied cases. The results reported in Figure 9 show how the $CO_2$ inventory variation is very limited if fixed pressures are assumed (CASE 3), while it can vary significantly if a sliding pressure at the turbine inlet is considered. CASE 3 scenario would thus imply smaller volumes required to store the excess $CO_2$ during part load operation.

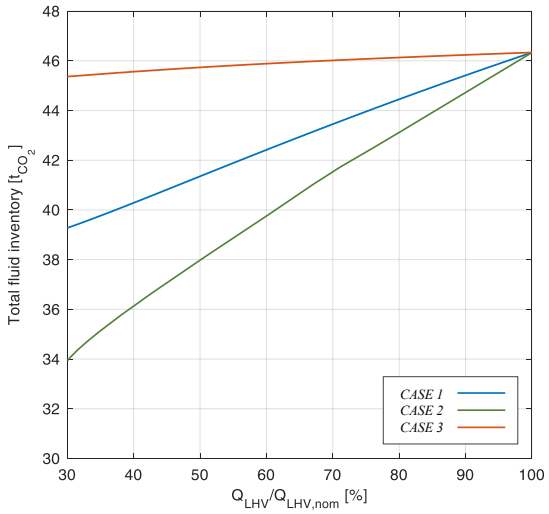


**Figure 9:** variation of $CO_2$ inventory within the system with the fuel input for the three different investigated strategies

## CONCLUSIONS AND FUTURE WORKS

In the present work, the study of a recuperative recompressed $sCO_2$ cycle with HTR by-pass as power cycle for a coal-fired power plant was performed. The achieved cycle efficiency is 41.92% and the overall plant efficiency is of about 39.56%. Once a preliminary design of all the main heat exchangers was performed, different part load operating strategies were compared in order to identify their impact on the plant efficiency and on the operating points of the main and secondary compressor. From the overall plant efficiency point of view keeping the same turbine inlet pressure at part load (thanks to IGV or partial arc admission) guarantees the best performance with an increase of plant efficiency at part load of 2.2 points percent thanks to the increased recuperators efficiency. This operating strategy guarantees also a limited $CO_2$ inventory variation, but on the other hand cannot be pursued with a single main compressor but requires more compressors in parallel. If the turbine works with sliding pressure the plant efficiency slightly increases down to 50% of the fuel input and then decreases and the $CO_2$ inventory changes significantly. With this operating strategy the optimization of the minimum cycle pressure has limited impact on the plant efficiency (0.7 points percent more at 30% of the fuel input) but can ease the operation of the main compressor. Future development of this work will include the study of the impact of the turbomachinery efficiency variation with the operating conditions and will investigate further operational degrees of freedom such as variation of the split ratio or of the HTR bypass ratio.

## NOMENCLATURE

### *Symbols*

| | |
|---|---|
| A | Area ($m^2$) |
| $c_p$ | Specific Heat Capacity (J/kg-K) |
| h | Enthalpy (J/kg-K) |
| htc | Heat Transfer Coefficient ($W/m^2$-K) |
| $k_t$ | Thermal Conductivity (W/mK) |
| $\dot{m}$ | Mass Flow Rate (kg/s) |
| $\dot{Q}$ | Thermal Power (W) |
| T | Temperature (°C) |
| U | Overall heat transfer coefficient ($W/m^2$-K) |
| $\dot{W}$ | Power (W) |
| $\eta$ | Efficiency (%) |
| $\xi$ | Specific HRU Elec. Consumption ($W_{el}/ W_{th}$) |
| Z | Compressibility factor |

### *Acronyms*

| | |
|---|---|
| APH | Air Preheater |
| BR | Bypass Ratio |
| HRU | Heat Rejection Unit |
| HTR | High Temperature Recuperator |
| HTRB | High Temperature Recuperator Bypass |
| HT-PHE | High Temperature Primary Heat Exchanger |
| HX | Heat Exchanger |
| LHV | Lower Heating Value |
| LTR | Low Temperature Recuperator |
| LT-PHE | Low Temperature Primary Heat Exchanger |
| PCHE | Printed Circuit Heat Exchanger |
| $SCO_2$ | Supercritical $CO_2$ |
| SR | Split Ratio |
| USC | Ultra Super Critical |
| VIGV | Variable Inlet Guide Vanes |

## ACKNOWLEDGEMENTS

The sCO2-flex project has received funding from the European Union's Horizon 2020 research and innovation programme under grant agreement N° 764690.
BHGE - Nuovo Pignone has provided preliminary turbomachinery information and parameters


DOI: 10.17185/duepublico/48897

**REFERENCES**


[1] "SCO2-flex." [Online]. Available: http://www.sco2-flex.eu/.

[2] G. Angelino, "Real gas effects in carbon dioxide cycles," in *International Gas Turbine Conference & products Show, Cleveland, Ohio - March 10-13, 1969*, 1969, no. ASME Paper No. 69-GT-102.

[3] F. Crespi, G. Gavagnin, D. Sánchez, and G. S. Martínez, "Supercritical carbon dioxide cycles for power generation: A review," *Appl. Energy*, vol. 195, pp. 152–183, 2017.

[4] D. Alfani, M. Astolfi, M. Binotti, S. Campanari, and P. Silva, "D5.1 - Report on the nominal design of different plant configurations and sensitivity analysis on main design parameters." 2019.

[5] Mathworks, "Matlab tool." Mathworks, 2017.

[6] E. Lemmon, M. Huber, and M. McLinden, "NIST standard reference database 23: reference thermodyanmi and transport properties-REFPROP." National Institue of Standards and Techology, Gaithersburg, 2013.

[7] M. Mecheri and S. Bedogni, "D1.3 - Report on the selected cycle architecture." 2018.

[8] "Thermoflow." 2016.

[9] V. Dostal, M. J. Driscoll, and P. Hejzlar, "Advanced Nuclear Power Technology Program A Supercritical Carbon Dioxide Cycle for Next Generation Nuclear Reactors," 2004.

[10] M. . Carlson, A. . Kruizenga, C. Schalansky, and D. F. Fleming, "Sandia progress on advanced heat exchangers for sCO2 Brayton cycles," in *The 4th International Symposium*, 2014.

[11] G. O. Musgrove, R. Le Pierres, and J. Nash, "Heat Exhangers for Supercritical CO2 Power Cycle Applications," in *The 4th International Symposium for Supercritical CO2 Power Cycles*, 2014.

[12] D. Alfani, M. Astolfi, M. Binotti, S. Campanari, F. Casella, and P. Silva, "Multi objective optimization of flexible supercritical CO2 coal-fired power plant," in *ASME Turbo Expo 2019: Turbomachinery technical conference and exibition*, 2019.

[13] T. L. Bergman and F. P. Incropera, *Fundamentals of heat and mass transfer.* Wiley, 2011.

[14] "LU-VE S.p.A. - Heat Exchangers for refrigeration and air conditioning." [Online]. Available: https://www.luve.it/. [Accessed: 30-Apr-2019].

[15] "Private communication with LU.VE." 2016.




DOI: 10.17185/duepublico/48897

**DOI:** 10.17185/duepublico/48897
**URN:** urn:nbn:de:hbz:464-20191002-160807-1